ISBN: 978-93-48091-58-1

3. Dielectric and Leakage Property Investigation in Lanthanum Doped $BiFeO_3$-$BaTiO_3$

Femina Brahma

Department of Physics,
Science College Kokrajhar, Kokrajhar, Assam.

S. Bhattacharjee

Department of Physics,
Kokrajhar Government College, Kokrajhar, Assam.

Santanu Sen, R. L. Hota, B. N. Parida

Department of Physics,
Central Institute of Technology Kokrajhar, BTR, Assam.

Abstract:

The new La doped $BiFeO_3$-$BaTiO_3$ perovskite-oriented material is synthesized through solid state reaction route technique at an optimized temperature 11000C. The structural investigation through XRD technique suggesting the phase of the material is tetragonal. The dielectric investigation through the shifting of tangent of loss and dielectric coefficient with frequency over a specific range of temperature gives indication of overall good dielectric feature of the material. Besides NTCR feature of the material is identifies through impedance spectroscopy. The leakage feature investigated through I-V characteristic technique suggesting good insulating property of the material for device-oriented application.

Keywords:

Perovskite; Dielectric; Leakage current; Semiconducting.

3.1 Introduction:

Now-a-days people are fond of smart materials. So, material scientists are also more interested on these materials for their fascinating characteristics. Perovskites are basically materials having the structure of ABO_3 which reflects very standard characteristics for the candidature of smart materials. Among all inorganic perovskites $BaTiO_3$ draws many attentions from material scientists for such kind of excellent behaviours. Lessening dielectric loss and improve the permittivity capacity, reduce the leakage current in perovskites many incorporations had been taken in the B-site and A-site respectively by cations of $BaTiO_3$ materials. In earlier works it has been detected that doping or the replacement of Zr^{4+} for Ti^{4+} in $BaTiO_3$ optimizes the leaky transportation assets and the dielectric trademarks (Chen et al., 2013).

To develop a multiferroic material perovskites are incorporated with several materials with magnetic ions in the recent past works either fully or partially. To build a multifunctional device these kinds of materials having more than one characteristic draws many attentions. Among the materials of multiferroics, perhaps the most appreciated kind is the $BiFeO_3$ (BFO), which conveys the ferroelectric behavior with curie temperature ~ 830^0C and anti-ferromagnetic with Neel temperature ~ 370^0C as per the literature survey. The $6s^2$ "lone pair" of the Bi^{3+} ions and the 3d electrons of the Fe^{3+} ions are liable for the ferroelectric and anti-ferromagnetic occurrences in the BFO as per the recent works (Zhang et al. 2016; Das et al., 2013). Alloys with a high constant of dielectric and low losses of dielectric serve as essentials for technologies as they make it feasible to develop components. This has been realised through the inclusion of Lanthanum Ferrite ($LaFeO_3$) Perovskite, also known as Orthoferrites, to $BaTiO_3$. Since orthoferrites feature outstanding magnetic attributes and minimal loss, the participation was decided upon for this cause (Das et al., 2013; Ranjan et al., 2016). Sorting of spin moments constitutes one of the many additional tangible advantages of orthoferrites. In contemplating this, further concurrently added Fe^{+3} and La^{+3} to $BaTiO_3$, yielding $(Bi_{0.75}La_{0.25}\ FeO_3)_{0.5}$- $(BaTiO_3)_{0.5}$ (LBF-BTO), and we inquired about its structural, dielectric, and leakage attributes.

3.2 Sample Preparation by The Solid Solution Synthesis Method:

The sample preparation task was approached via the solid oxide, adopted to create the polymorphic sample $(Bi_{0.75}\ La_{0.25}\ FeO_3)_{0.5}$-$(BaTiO_3)_{0.5}$ (BLF-BTO) adopting the appropriate proportions of the unprocessed components La_2O_3, $BaCO_3$, TiO_3, Bi_2O_3, and Fe_2O_3. The exorbitant amount-pure elements (>99%), picked from the manufactures of loba chemicals. The formula for chemical reactions, outlined underneath was put to use to generate the currently used compound.

$$\mathbf{0.25\ La_2O_3 + 0.75Bi_2O_3 + Fe_2O_3 + 2\ BaCO_3 + 2\ TiO_2 \rightarrow 4\ (Bi_{0.75}La_{0.25}\ FeO_3)_{0.5}\text{-}(BaTiO_3)_{0.5} + 2\ CO_2}$$

The abovementioned ingredients are first dry grinded for about 1 hour and then wet grinded in methanol for another 1 hour. The prepared sample was heated in high temperature furnace and the sample was formed at 1100 ^{0}C. The X-ray Diffraction analysis gives the assurance for the formation of the required compound, the solid solution of the material was palletized in the form of disc with the thickness of nearly 3 mm and diameter of 10mm, with polyvinyl Chloride and sintered at around 1150 ^{0}C for another 6 hours. The dielectric properties and I-V characteristics of the material is performed in the LCR meter for the frequency from 100 Hz to 5 MHz in the temperature range of room temperature to 500 ^{0}C.

3.3 Results and Discussions:

3.3.1 Structure and Microstructure Study:

The XRD pattern as shown in the Fig. 3.1 indicates that there are number of sharp peaks at defined different Bragg's angles similar to raw material which confirms the formation of single-phase new compound. The produced sample fits nicely into the orthorhombic structure after analysis in the "POWD" software. The projected unit cell encompasses the

following probable values: a = 21.5828; b = 3.9744; c/a = 0.1841; and V = 1851.33; with a standard variance of 0.0031. Utilizing the Debye-Scherer formula, the cell/crystallite dimension of the LBF-BTO sample was determined to be 23 nm.

$$D_{hkl} = k\lambda/\beta cos\theta_{hkl}$$

where k = constant = 0.89, λ = 1.54050 A^0 and = full width at half maximum.

Tolerance factor is calculated using formula

$$t' = \frac{(r_A + r_o)}{\sqrt{2}(r_B + r_{O)}}$$

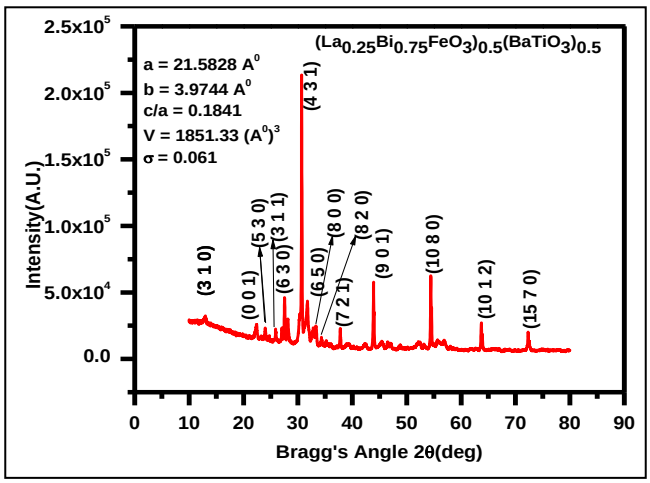

Figure 3.1: Shows the XRD pattern of the studied sample.

where r_A, r_B, and r_O are the cations' ionic radiuses, respectively, for the A, B, and oxygen anions (in Å unit), and it is found to be <1 which confirms that all structures are distorted from the ideal cubic symmetry.

3.3.2 Frequency Dependent Dielectric Properties:

Figure 3.2 shows the dielectric (ε_r) property with frequency. The material's dielectric capability diminishes as frequency climbs and peaks in low frequency. High capacitance levels arise from polarisation at the junction, and low levels emerge as frequency-dependent improper alignment or phase mismatch of the dipoles occurs relative to local relative to the local pinning field direction. As shown in the Figure 3.3 the dielectric loss or tan delta with frequency, it is predicted that at low frequency there is a relaxation peak with temperature and at high frequency the loss is low for every temperature variation. At lower frequency as the charge carriers require high energy to cross barrier of grain boundary results in high resistance and due to it the high loss but as the frequency raised the low resistance offered by grains gives the low value of loss wang

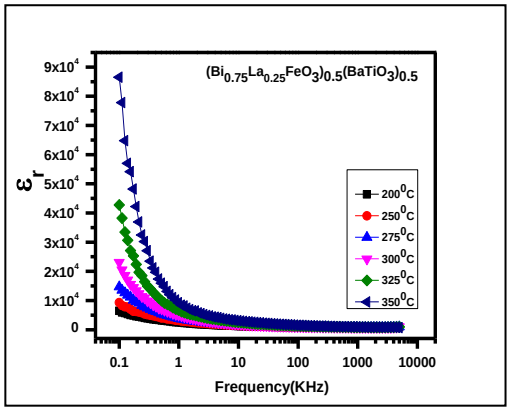

Figure 3.2: Variation of dielectric. and frequency

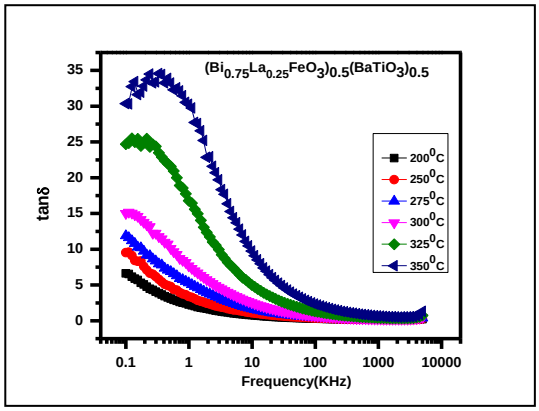

Figure 3.3: Tangent loss variation with frequency

3.3.3 Complex Impedance and Modulus Studies:

To analyse the electrical properties, impedance analysis is the most important tool. This analysis gives us the understanding of the contributions from the material's electrode, intra-, and inter-grain impacts. $Z^*(\omega) = Z' + jZ''$ represents the complex impedance spectroscopy, and Z' and Z'' represent the real and imaginary parts of the complex impedance, respectively (Mohanty et al., 2020; Wang et al., 2020).

To analyze electrical properties PSM-1735,4NL-LCR, UK. The electrical measurement was taken in wide range of frequencies from 100 Hz to 5 MHz and temperature in the range of 25–500 °C. The real part of the complex impedance (Z') varying with frequency at different temperatures in the interval of 5^0C in the range of 25^0 to 500^0C is shown in the fig. 3.4. This behavior is termed as Negative Temperature Coefficient of Resistance (NTCR) in the material. The release of space charges at grain boundaries gives a decreasing and merge curves at high frequencies for all the temperatures.

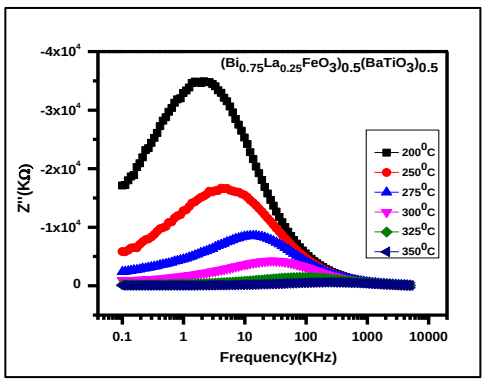

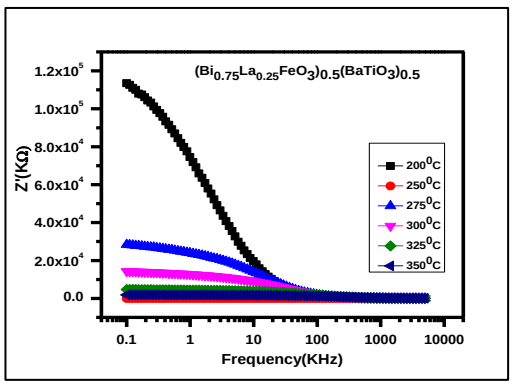

Figure 3.4: Variation of Z' with frequency. Figure 3.5: Variation of Z'' with frequency

The relaxed response of the material is determined by the shift of the imaginary component of impedance (Z") with a specified range of temperatures and frequency. Grain boundaries add to the ridges in the lower part of the frequency, while grain is liable for the flattened part of the higher frequency. Consequently, the reduced temperature relaxation in these specimens originates from stagnant charges, unexplained imperfections and vacancies in oxygen leading to in elevated temperature relaxation (Ranjan et al., 2011; Aliouane et al., 2005; Wang et al., 2002).

3.3.4 Leakage Property Studies:

The Figure 3.6 indicates the Current(I) and Voltage (V) variation in the range of 25^0C to 325^0C. Current (I) -Voltage(V) characteristic gives us the information regarding the leakage current and types of charge carriers The leakage feature investigated through I-V characteristic technique suggesting good insulating property of the material for device fabrication application. The leakage current is increasing with the increment of voltage. But it was observed that with respect to increase in temperature the leakage current goes in decreasing. To understand the leakage-current properties

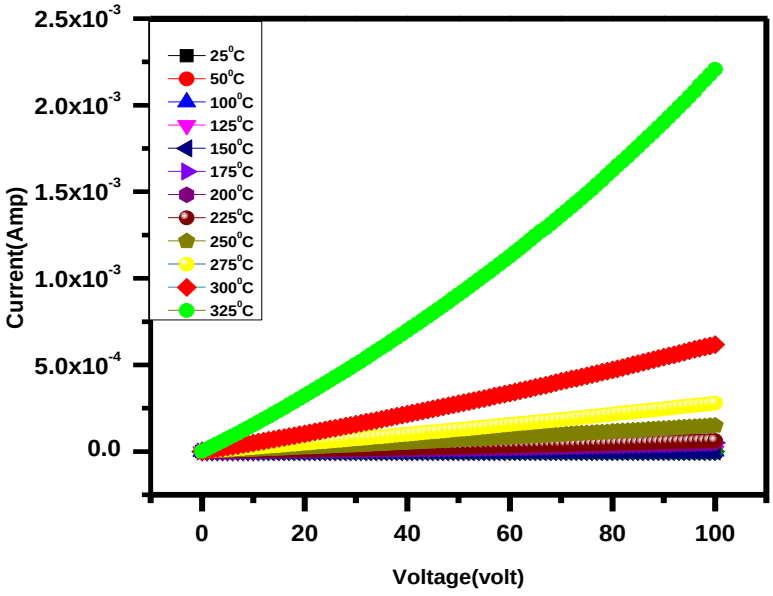

Figure 3.6: Shows Variation of Current with Voltage

we have to consider various types of conduction phenomena like (i) interface-limited conduction phenomena and (ii) bulk-limited conduction phenomena. The interface-limited phenomena originated from the difference in Fermi levels between a metal and an insulator or a semiconductor. The energy difference produces a potential barrier between the metal and the insulator, charges must overcome it and leakage takes place (Das et al., 2019). But it was observed that with increase in temperature the leakage current goes in decreasing. Besides it, non-linearity behavior observed in the leakage current curve with temperature suggests the n-type semi-conducting feature of the material.

3.4 Conclusion:

BFO-BTO was successfully synthesized in the solid oxide root method which was confirm through XRD diffraction characterization. The material formed in the single phase, having orthorhombic crystal structure. The material has good dielectric property along with low tangent loss. The NTCR behavior was confirmed through impedance analysis. The I-V curves confirmed the low leakage property of the material and also it gives us the information regarding charge carriers. The material is free of lead. So, the device which will be fabricated with the synthesized material is good for sustainable environment.

Declaration of Competing Interest:

The authors declare that they have no known competing financial interest's personal relationships that could have appeared to influence the work reported in this paper.

3.5 References:

1. Chen, K., Liu, M., Liu, Y., Wang, C., Yoshimura, T., Gong, W., ... & Wang, J. M. (2013). 42: Signal relay by CCR2 and formylpeptide receptor-2 (Fpr2) in the recruitment of monocyte-derived dendritic cells in allergic airway inflammation. *Cytokine*, *63*(3), 253.
2. Prosposito, P., Burratti, L., & Venditti, I. (2020). Silver nanoparticles as colorimetric sensors for water pollutants. *Chemosensors*, *8*(2), 26.
3. BelBruno, J. J. (2013). Nanomaterials in sensors. *Nanomaterials*, *3*(4), 572-573.
4. Zhang, W., Eperon, G. E., & Snaith, H. J. (2016). Metal halide perovskites for energy applications. *Nature Energy*, *1*(6), 1-8.
5. Gao, P., Grätzel, M., & Nazeeruddin, M. K. (2014). Organohalide lead perovskites for photovoltaic applications. *Energy & Environmental Science*, *7*(8), 2448-2463.
6. Varignon, J., Bibes, M., & Zunger, A. (2019). Origin of band gaps in 3 d perovskite oxides. *Nature communications*, *10*(1), 1658.
7. Zhang, J., Qin, Z., Zeng, D., & Xie, C. (2017). Metal-oxide-semiconductor based gas sensors: screening, preparation, and integration. *Physical Chemistry Chemical Physics*, *19*(9), 6313-6329.
8. Das, P. R., Parida, B. N., Padhee, R., & Choudhary, R. N. P. (2013). Electrical properties of $Na_2Pb_2R_2W_2Ti_4V_4O_{30}$(R= Dy, Pr) ceramics. *Journal of Advanced Ceramics*, *2*, 112-118.
9. Brahma, F., Mohanty, B., Bhattacharjee, S., Hota, R. L., Parida, R. K., & Parida, B. N. (2021). Investigation of multifunctional characteristics in $SmFeO_3$-$BaTiO_3$ perovskite system for devices. *Materials Science in Semiconductor Processing*, *135*, 106071.
10. Aliouane, K., Guehria-Laidoudi, A., Simon, A., & Ravez, J. (2005). Study of new relaxor materials in $BaTiO_3BaZrO_3La_2/3TiO_3$ system. *solid state sciences*, *7*(11), 1324-1332.
11. Wang, Y., Li, L., Qi, J., & Gui, Z. (2002). Ferroelectric characteristics of ytterbium-doped barium zirconium titanate ceramics. *Ceramics international*, *28*(6), 657-661.
12. Chou, X., Zhai, J., Jiang, H., & Yao, X. (2007). Dielectric properties and relaxor behavior of rare-earth (La, Sm, Eu, Dy, Y) substituted barium zirconium titanate ceramics. *Journal of Applied Physics*, *102*(8).

13. Hao, S. E., Sun, L., & Huang, J. X. (2008). Preparation and dielectric properties of Dy, Er-doped BaZr0. 2Ti0. 8O3 ceramics. *Materials Chemistry and Physics*, *109*(1), 45-49.
14. Zhang, Q., Cai, W., Li, Q., Gao, R., Chen, G., Deng, X., ... & Fu, C. (2019). Enhanced piezoelectric response of (Ba,Ca)(Ti,Zr)O_3 ceramics by super large grain size and construction of phase boundary. *Journal of Alloys and Compounds*, *794*, 542-552.
15. Catalan, G., & Scott, J. F. (2009). Physics and applications of bismuth ferrite. *Advanced materials*, *21*(24), 2463-2485.
16. Kenzelmann, M., Harris, A. B., Jonas, S., Broholm, C., Schefer, J., Kim, S. B., ... & Lynn, J. W. (2005). Magnetic inversion symmetry breaking and ferroelectricity in TbMnO 3. *Physical review letters*, *95*(8), 087206.
17. Mohanty, B., Parida, B. N., & Parida, R. K. (2020). Structural, dielectric and magnetic behavior of BST modified rare earth ortho-ferrite $LaFeO_3$. *Ceramics International*, *46*(10), 16502-16509.
18. Wang, T., Liu, J., Kong, L., Yang, H., Wang, F., & Li, C. (2020). Evolution of the structure, dielectric and ferroelectric properties of $Na_{0.5}Bi_{0.5}TiO_3$-added $BaTiO_3$–$Bi(Mg_{2/3}Nb_{1/3})O_3$ ceramics. *Ceramics International*, *46*(16), 25392-25398.
19. Brahma, F., Mohanty, B., Bhattacharjee, S., Hota, R. L., Parida, R. K., & Parida, B. N. (2021). Investigation of multifunctional characteristics in $SmFeO_3$-$BaTiO_3$ perovskite system for devices. *Materials Science in Semiconductor Processing*, *135*, 106071.
20. Brahma, F., Hota, R. L., Parida, R. K., & Parida, B. N. (2022). Structural and electrical investigation of 'Bi'doped SmFeO3-BaTiO3 perovskite system. *Materials Today: Proceedings*, *49*, 2365-2368.
21. Das, R., & Choudhary, R. N. P. (2019). Structural, electrical, and leakage-current characteristics of double perovskite: Sm_2CoMnO_6. *Applied Physics A*, *125*(12), 864.